

# Extended Black Hole Solutions in Rastall Theory of Gravity

M. Sharif<sup>1</sup> \* and M. Sallah<sup>1,2</sup> †

<sup>1</sup> Department of Mathematics and Statistics, The University of Lahore  
1-KM Defence Road Lahore-54000, Pakistan.

<sup>2</sup> Department of Mathematics, The University of The Gambia,  
Serrekunda, P.O. Box 3530, The Gambia.

## Abstract

We utilize the gravitational decoupling via the extended geometric deformation to extend the Schwarzschild vacuum solution to new black holes in Rastall theory. By employing linear transformations that deform both the temporal and radial coefficients of the metric, the field equations with a dual matter source are successfully decoupled into two sets. The first of these sets is described by the metric for the vacuum Schwarzschild spacetime, while the second set corresponds to the added extra source. Three extended solutions are obtained using two restrictions on the metric potentials and extra source, respectively. For selected values of the Rastall and decoupling parameters, we study the impact of the fluctuation of these parameters on the obtained models. We also investigate the asymptotic flatness of the resulting spacetimes by analysis of the metric coefficients. Finally, the nature of the additional source is explored for each model, via analysis of the energy conditions. It is found among other results that none of the obtained models satisfy the energy conditions, while only the model corresponding to the barotropic equation of state mimics an asymptotically flat spacetime.

---

\*msharif.math@pu.edu.pk

†malick.sallah@utg.edu.gm

**Keywords:** Rastall gravity; Gravitational decoupling; Killing horizon; Causal horizon.

**PACS:** 04.50.Kd; 04.40.Dg; 04.40.-b.

## 1 Introduction

The assumption behind the Rastall theory of gravity [1] is that the laws of conservation such as the conservation of mass and energy can only be studied within the flat or weak-field domain of spacetime. Recently, a novel idea has been put forth which introduces the non-minimal interaction between matter and gravitational fields as the source of the universe accelerating momentum [2]. Rastall argument allows one to add new elements to the Einstein field equations by relaxing the requirement that the covariant derivative of the energy-momentum tensor be zero. Indeed, it has recently been demonstrated that in a curved spacetime, the divergence of the energy-momentum tensor can be non-zero [3]. Numerous precise solutions have been found for this theory in both astrophysical [4]-[8] and cosmological contexts [9]-[13].

By contrasting the thermodynamic quantities and features of black holes in Rastall gravity with those found in general relativity (GR), the Rastall hypothesis allows us to better appreciate the quality of the connection between geometry and matter fields, which is non-minimal. The Einstein field equations produce numerous solutions that exhibit the geometric structure of spacetime. An object known as a black hole (a region of spacetime with a coordinate singularity given by an event horizon, beyond which nothing escapes its strong gravitational pull) is the result of many solutions of the Einstein field equations. Some well-known black hole solutions are developed by Schwarzschild, Riessner-Nordstrom, Kerr and Kerr-Newmann. Apart from the theoretical descriptions, gravitational waves resulting from the merger of two black holes have been observed by LIGO [14], and the event horizon telescope has recently obtained the first-ever actual image of a black hole [15]. Black hole solutions including but not limited to the static black hole [16] and the rotating charged black hole solutions [17], have been found in Rastall theory. The thermodynamics of black holes in Rastall gravity have also been studied [18].

To create new models of relativistic objects with unique properties, Ovalle introduced the gravitational decoupling technique [19]. In many situations [20]-[24], this technique has shown to be a useful theoretical method for con-

structuring potential star distributions. Many authors [25] used this procedure to describe the inner region of self-gravitating compact structures with both exotic as well as realistic fluids having anisotropic distributions. Due to the extreme nonlinearity of the field equations, there are relatively few physically sound analytical solutions accessible, unless there are very particular constraints. The division of the source energy-momentum into two halves is the foundation of the gravitational decoupling extension. The first is selected to produce a known solution of GR, while the second one relates to an extra source that may contain any kind of charge, such as gauge and tidal charges, or hairy fields related to gravity outside of GR.

The gravitational decoupling technique, however, comes in two folds viz the minimal geometric deformation (MGD) and the extended geometric deformation (EGD). The fundamental difference between the MGD and EGD is that the former transforms only the  $g_{rr}$  component of the spacetime metric while the latter transforms both the  $g_{tt}$  and  $g_{rr}$  metric coefficients of the spacetime. Additionally, the MGD is limited in that it only applies when the decoupled sources have a strictly gravitational interaction. This implies that it is inapplicable in a scenario where there is energy exchange between the decoupled sources. Using the deformation on both temporal and radial metric functions, Casadio et al. [26] proposed an enhanced version of the MGD approach to address this problem and produced a new solution for spherically symmetric spacetime. However, since the conservation law breaks down in the presence of matter, this extension is limited to studying vacuum solutions. As such, this extended technique cannot be used to discuss the intrinsic features and internal structure of self-gravitating objects. Despite the said limitations, the MGD approach has in recent time registered great success in obtaining anisotropic solutions to different realistic compact stellar configurations in GR [27] as well as in various modified theories [28], including the Rastall theory [29]. With regards to black holes, we have used the MGD scheme to extend the well known regular Hayward and Bardeen black hole solutions in Rastall theory [30]. Furthermore, Ovalle has used the MGD decoupling to extend the Schwarzschild black hole in GR [31].

By altering both metric potentials, Ovalle [32] introduced the innovative concept of EGD, which is applicable throughout spacetime and is independent of the choice of matter distribution. The EGD has since been exploited by numerous researchers to derive anisotropic spherical solutions in a cascade of alternative theories. Contreras and Bargueno applied the EGD scheme to vacuum BTZ solution in  $2 + 1$ -dimensions [33]. Sharif and Mughani [34] used

the same scheme and extended the Tolman IV and Krori-Barua solutions, respectively, to derive anisotropic solutions. Sharif and Majid [35] found extended gravitationally decoupled solutions of the Krori-Barua and Tolman IV ansatz in self-interacting Brans-Dicke theory. Ovalle and his collaborators [36] exploited this scheme to obtain hairy black holes by extending the vacuum Schwarzschild spacetime. Sharif and Majid [37] explored the effects of charge on decoupled solutions in self-interacting Brans-Dicke (BD) theory by taking Tolman IV and Krori-Barua solutions. The same authors [38] used the EGD method to extend the vacuum Schwarzschild black hole in BD theory. Sharif and Naseer [39] investigated extended decoupled anisotropic solutions in  $f(\mathcal{R}, T, \mathcal{R}_{ab}T^{ab})$  theory, using the EGD technique both in the presence and absence of charge. The same authors [40] utilized this procedure to investigate its effects on isotropization and complexity in  $f(\mathcal{R}, T)$  theory. They [41] also investigated the effect of charge on complexity and isotropization of extended decoupled anisotropic stellar models in the same theory.

In this work, we exploit the EGD approach to extend the vacuum Schwarzschild black hole in Rastall theory. We obtain three generalized solutions which we study in great detail and compare with the earlier literature. The rest of this paper is aligned as follows. Section 2 outlines the Rastall field equations for a dual matter source and consequently defines some effective parameters. We then apply the EGD technique to the field equations (Section 3). In Section 4, we derive three extended solutions and interpret these solutions via analysis of the deformed metric potentials, the effective thermodynamic variables and the energy conditions. Finally, we summarize our findings in a well-articulated conclusion, in Section 5.

## 2 Rastall Field Equations

The Rastall field equations are discriminated from the field equations of GR through the Rastall parameter  $\lambda$  which also relates the covariant divergence of the Rastall stress-energy tensor to that of the curvature scalar,  $\mathcal{R}$ . The field equations for the Rastall theory can be formulated as

$$G_{ab} + \frac{\lambda}{4}\mathcal{R}g_{ab} = \kappa T_{ab}^R, \quad (1)$$

where

$$\nabla^b T_{ab}^R = \frac{\lambda}{4} g_{ab} \nabla^b \mathcal{R}, \quad (2)$$

describes the covariant divergence of the Rastall stress-energy tensor  $T_{ab}^R$ . From Eq.(1),  $G_{ab}$  denotes the Einstein tensor while  $g_{ab}$  and  $\kappa$  denote the metric tensor and coupling constant, respectively.

The field equations (1) can be expressed in the alternate form

$$G_{ab} = \kappa \left( T_{ab}^R - \frac{\lambda}{4(\lambda - 1)} T^R g_{ab} \right), \quad (3)$$

by contracting them and using the resulting expression for the curvature scalar  $\mathcal{R}$ . Equation (3) can be written as

$$G_{ab} = \kappa T_{ab}, \quad (4)$$

if we define

$$T_{ab} = T_{ab}^R - \frac{\lambda}{4(\lambda - 1)} T^R g_{ab}. \quad (5)$$

This reorganization wherein the nonconforming terms of the Einstein tensor are grouped, leading to the formation of an effective stress-energy tensor, can be performed in any modified theory irrespective of the state of conservation of their stress-energy tensor. With this effective stress-energy tensor, the usual conservation result  $\nabla^b T_{ab} = 0$  is regained. If we identify  $T_{ab}$  as the perfect fluid isotropic energy-momentum tensor of GR, expressed as

$$T_{ab} = (\rho + P) u_a u_b - P g_{ab}, \quad (6)$$

with  $\rho$ ,  $P$ ,  $u_a = \sqrt{g_{00}} \delta_a^0$  denoting the density, isotropic pressure, and 4-velocity, respectively, then Eq.(5) relates the energy-momentum tensors of the GR and Rastall theories. Further contracting Eq.(5) gives the explicit relationship

$$(1 - \lambda) T = T^R, \quad (7)$$

between  $T$  and  $T^R$ , the traces of the GR and Rastall stress-energy tensors, respectively. By this relation, the Rastall stress-energy tensor can be expressed as

$$T_{ab}^R = T_{ab} - \frac{\lambda}{4} T g_{ab}. \quad (8)$$

In order to use the gravitational decoupling technique to extend a known solution, we consider the field equations (1) with the modification

$$G_{ab} + \frac{\lambda}{4}\mathcal{R}g_{ab} = \kappa T_{ab}^{(total)}, \quad (9)$$

where

$$T_{ab}^{(total)} = T_{ab}^R + \beta\Theta_{ab}. \quad (10)$$

Equation (10) shows that the total energy-momentum tensor comprises a seed source ( $T_{ab}^R$ ) to which an extra matter source ( $\Theta_{ab}$ ) is gravitationally coupled via the decoupling parameter,  $\beta$ . This extra source may contain new fields of scalars, vectors, and tensors and it is responsible for generating anisotropy in the fluid. This total energy-momentum tensor must (owing to its definition) satisfy the conservation equation

$$T_{b;a}^{a(total)} = 0. \quad (11)$$

We employ the following static spherically symmetric metric to describe our spacetime geometry

$$ds^2 = e^{a(r)}dt^2 - e^{b(r)}dr^2 - r^2(d\theta^2 + \sin^2\theta d\phi^2). \quad (12)$$

This metric satisfies the field equations (1), given by the system below

$$\begin{aligned} \kappa \left[ \rho - \frac{\lambda}{4}(\rho - 3P) + \beta\Theta_0^0 \right] &= \frac{1}{r^2} + e^{-b} \left( \frac{b'}{r} - \frac{1}{r^2} \right) + \frac{\lambda e^{-b}}{4} \left( a'' + \frac{a'(a' - b')}{2} \right) \\ &+ \frac{\lambda e^{-b}}{4} \left( \frac{2(a' - b')}{r} + \frac{2}{r^2} \right) - \frac{\lambda}{2r^2}, \end{aligned} \quad (13)$$

$$\begin{aligned} \kappa \left[ P + \frac{\lambda}{4}(\rho - 3P) - \beta\Theta_1^1 \right] &= -\frac{1}{r^2} + e^{-b} \left( \frac{a'}{r} + \frac{1}{r^2} \right) - \frac{\lambda e^{-b}}{4} \left( a'' + \frac{a'(a' - b')}{2} \right) \\ &- \frac{\lambda e^{-b}}{4} \left( \frac{2(a' - b')}{r} + \frac{2}{r^2} \right) + \frac{\lambda}{2r^2}, \end{aligned} \quad (14)$$

$$\kappa \left[ P + \frac{\lambda}{4}(\rho - 3P) - \beta\Theta_2^2 \right] = e^{-b} \left( \frac{a''}{2} + \frac{(a')^2}{4} - \frac{a'b'}{4} + \frac{a'}{2r} - \frac{b'}{2r} \right) + \frac{\lambda}{2r^2}$$

$$-\frac{\lambda e^{-b}}{4} \left( a'' + \frac{a'(a' - b')}{2} + \frac{2(a' - b')}{r} + \frac{2}{r^2} \right). \quad (15)$$

The conservation equation (11) with respect to the system above is given as

$$\frac{dP(r)}{dr} + \frac{a'(r)}{2}(\rho + P) + \frac{2\beta}{r}(\Theta_2^2 - \Theta_1^1) + \frac{\beta a'(r)}{2}(\Theta_0^0 - \Theta_1^1) - \beta \left( \Theta_1^1(r) \right)' = 0. \quad (16)$$

This system comprises three nonlinear ordinary differential equations in the seven unknowns  $a(r)$ ,  $b(r)$ ,  $\rho(r)$ ,  $P(r)$ ,  $\Theta_0^0$ ,  $\Theta_1^1$ ,  $\Theta_2^2$ , and  $' = \frac{d}{dr}$ . It is from this system that the following effective parameters are identified

$$\rho^{eff} = \rho + \beta \Theta_0^0, \quad P_r^{eff} = P - \beta \Theta_1^1, \quad P_t^{eff} = P - \beta \Theta_2^2. \quad (17)$$

These effective parameters imply an anisotropy induced by the extra source  $\Lambda_{ab}$ , given by

$$\Delta^{eff} = P_t^{eff} - P_r^{eff} = \beta(\Theta_1^1 - \Theta_2^2), \quad (18)$$

which vanishes only in the event  $\Theta_1^1 = \Theta_2^2$ .

### 3 Extended Geometric Deformation Technique

In a bid to solve the system (13)-(15), we employ the EGD technique which deforms both the temporal and radial metric coefficients by means of some appropriate linear transformations. Using these transformations, the system splits into two sets, the first of which corresponds to a perfect fluid matter distribution ( $\beta = 0$ ). The second set entails the additional source  $\Lambda_{ab}$  and depicts a quasi-Einstein system. Proceeding, we consider a known ideal fluid solution to the field equations, described by the metric

$$ds^2 = e^{\sigma(r)} dt^2 - \frac{1}{\eta(r)} dr^2 - r^2(d\theta^2 + \sin^2 \theta d\phi^2), \quad (19)$$

with

$$\eta(r) = 1 - \frac{2m(r)}{r}, \quad (20)$$

where  $m$  represents the Misner-Sharp mass. The linear transformations that characterize the geometric deformation are given by

$$\sigma(r) \mapsto a(r) = \sigma(r) + \beta f_1(r), \quad \eta(r) \mapsto e^{-b(r)} = \eta(r) + \beta f_2(r), \quad (21)$$

where  $f_1(r)$  and  $f_2(r)$  denote the deformations applied to the temporal and radial metric components, respectively. Substituting the transformations (21) into the field equations, we obtain the first set as

$$\begin{aligned} \kappa \left[ \rho - \frac{\lambda}{4}(\rho - 3P) \right] &= \eta \left( \frac{\lambda\sigma''}{4} - \frac{1}{r^2} + \frac{\lambda(\sigma')^2}{8} + \frac{\lambda\sigma'}{2r} + \frac{\lambda}{2r^2} \right) \\ &+ \eta' \left( \frac{\lambda}{2r} + \frac{\lambda\sigma'}{8} - \frac{1}{r} \right) - \frac{\lambda}{2r^2} + \frac{1}{r^2}, \end{aligned} \quad (22)$$

$$\begin{aligned} \kappa \left[ P + \frac{\lambda}{4}(\rho - 3P) \right] &= \eta \left( \frac{\sigma'}{r} - \frac{\lambda\sigma''}{4} + \frac{1}{r^2} - \frac{\lambda(\sigma')^2}{8} - \frac{\lambda\sigma'}{2r} - \frac{\lambda}{2r^2} \right) \\ &- \eta' \left( \frac{\lambda\sigma'}{8} + \frac{\lambda}{2r} \right) + \frac{\lambda}{2r^2} - \frac{1}{r^2}, \end{aligned} \quad (23)$$

$$\begin{aligned} \kappa \left[ P + \frac{\lambda}{4}(\rho - 3P) \right] &= \eta \left( \frac{\sigma''}{2} + \frac{(\sigma')^2}{4} + \frac{\sigma'}{2r} - \frac{\lambda\sigma''}{4} - \frac{\lambda(\sigma')^2}{8} - \frac{\lambda\sigma'}{2r} - \frac{\lambda}{2r^2} \right) \\ &+ \eta' \left( \frac{\sigma'}{4} + \frac{1}{2r} - \frac{\lambda\sigma'}{8} - \frac{\lambda}{2r} \right) + \frac{\lambda}{2r^2}, \end{aligned} \quad (24)$$

associated to the conservation equation

$$\frac{dP(r)}{dr} + \frac{a'(r)}{2}(\rho + P) = 0. \quad (25)$$

By adopting any known spherically symmetric solution for the metric potentials ( $\sigma$  and  $\eta$ ) and expressing the density and pressure in terms of these metric potentials, the system Eqs.(22)-(24) can be solved.

The second set is given by the following system

$$\begin{aligned} \kappa(\Theta_0^0) &= \frac{\lambda}{4} \left[ f_2 \left( \sigma'' + \frac{(\sigma')^2}{2} + \frac{2\sigma'}{r} \right) + f_2' \left( \frac{\sigma'}{2} + \frac{2}{r} \right) + \eta f_1'' + \eta \sigma' f_1' + \frac{\eta \beta (f_1')^2}{2} \right. \\ &\left. + \frac{\eta' f_1'}{2} + \frac{2\eta f_1'}{r} \right] - \frac{f_2'}{r} - \frac{f_2}{r^2}, \end{aligned} \quad (26)$$

$$\kappa(\Theta_1^1) = \frac{\lambda}{4} \left[ f_2 \left( \sigma'' + \frac{(\sigma')^2}{2} + \frac{2\sigma'}{r} \right) + f_2' \left( \frac{\sigma'}{2} + \frac{2}{r} \right) + \eta f_1'' + \eta \sigma' f_1' + \frac{\eta \beta (f_1')^2}{2} \right]$$



$$+ \frac{\eta' f_1'}{2} + \frac{2\eta f_1'}{r} \Big] - f_2 \left( \frac{\sigma'}{r} + \frac{1}{r^2} \right) - \frac{\eta f_1'}{r}, \quad (27)$$

$$\begin{aligned} \kappa(\Theta_2^2) &= \frac{\lambda}{4} \left[ f_2 \left( \sigma'' + \frac{(\sigma')^2}{2} + \frac{2\sigma'}{r} \right) + f_2' \left( \frac{\sigma'}{2} + \frac{2}{r} \right) + \eta f_1'' + \eta \sigma' f_1' + \frac{\eta \beta (f_1')^2}{2} \right. \\ &+ \frac{\eta' f_1'}{2} + \frac{2\eta f_1'}{r} \Big] - f_2 \left( \frac{\sigma''}{2} + \frac{(\sigma')^2}{4} + \frac{\sigma'}{2r} \right) - f_2' \left( \frac{\sigma'}{4} + \frac{1}{2r} \right) - \frac{\eta' f_1'}{4} \\ &- \eta \left( \frac{f_1''}{2} + \frac{\beta (f_1')^2}{4} + \frac{\eta' f_1'}{2} + \frac{f_1'}{2r} \right), \end{aligned} \quad (28)$$

and conserves according to the equation

$$\frac{2\beta}{r} (\Theta_2^2 - \Theta_1^1) + \frac{\beta a'(r)}{2} (\Theta_0^0 - \Theta_1^1) - \beta \left( \Theta_1^1(r) \right)' = 0. \quad (29)$$

The system (26)-(28) above is solved by imposing two constraints (as there are five unknowns in three equations). The first of these constraints will be applied to the metric potentials while the second will be imposed on the extra source via a linear equation of state (EoS). A solution to the field equations (13)-(15) is thus found by the superposition principle, via a combination of the solutions of the two systems above, such as given by Eq.(17).

## 4 Extended Schwarzschild Solutions

Here, we develop from the results of the previous section and obtain the deformation functions  $f_1(r)$  and  $f_2(r)$  for the Schwarzschild vacuum solution, given by

$$ds^2 = \left( 1 - \frac{2M}{r} \right) dt^2 - \left( 1 - \frac{2M}{r} \right)^{-1} dr^2 - r^2 d\theta^2 - r^2 \sin^2 \theta d\phi^2, \quad (30)$$

where  $M$  denotes the Schwarzschild mass. Due to the presence of a vacuum, we have  $\rho = P = 0$ , thus redefining the effective parameters in Eq.(17). The transformations in Eq.(21) deform the Schwarzschild metric as follows

$$ds^2 = \left( 1 - \frac{2M}{r} \right) e^{\beta f_1(r)} dt^2 - \frac{dr^2}{\left( 1 - \frac{2M}{r} + \beta f_2(r) \right)} - r^2 \left( d\theta^2 + \sin^2 \theta d\phi^2 \right), \quad (31)$$

yielding the extended Schwarzschild solution. From the Schwarzschild metric (30), we observe the overlap of the Killing ( $r_H$ ) and the causal horizons ( $r_h$ ), at the surface  $r = 2M$ . These horizons are determined by  $e^a = 0$  and  $e^{-b} = 0$ , respectively [30]. It can also be observed that there lies a singularity at  $r = 0$ , behind the Killing and causal horizons. By the coincidence of these, a prerequisite is obtained for the EGD metric (31) to depict a well-defined black hole. This coincidence implies that  $e^a = e^{-b}$ , which yields the first constraint

$$a = -b. \quad (32)$$

Using this constraint in the transformation equations (21), we obtain the fundamental relationship between the deformation functions, given by

$$f_2(r) = \frac{(r - 2M)(e^{\beta f_1(r)} - 1)}{\beta r}. \quad (33)$$

The second constraint needed to evaluate the deformation functions  $f_1$  and  $f_2$  is given via the following linear EoS [30]

$$\Theta_0^0 + \alpha_1 \Theta_1^1 = \alpha_2 \Theta_2^2, \quad (34)$$

with  $\alpha_1$  and  $\alpha_2$  are arbitrary constants.

Following are three extensions of the Schwarzschild black hole, each of which is obtained using a particular case of the EoS (34).

#### 4.1 Model I: Traceless $\Theta_b^a$

Since  $\Theta_2^2 = \Theta_3^3$ , it is reasonable to assume that the extra source has a trace-free energy-momentum tensor when  $\alpha_1 = 1$  and  $\alpha_2 = -2$  in (34), i.e.,

$$\Theta_0^0 + \Theta_1^1 = -2\Theta_2^2. \quad (35)$$

Utilizing the system (26)-(28), Eq.(35) becomes

$$\begin{aligned} & -f_2 \left( \frac{\sigma'}{r} + \frac{2}{r^2} \right) - \frac{f_2'}{r} - \frac{\eta f_1'}{r} + \lambda \left[ f_2 \left( \sigma'' + \frac{\sigma'^2}{2} + \frac{2\sigma'}{r} \right) + f_2' \left( \frac{\sigma'}{2} + \frac{2}{r} \right) + \eta f_1'' \right. \\ & \left. + \eta \sigma' f_1' + \frac{\eta \beta f_1'^2}{2} + \frac{\eta' f_1'}{2} + \frac{2\eta f_1'}{r} \right] - f_2 \left( \sigma'' + \frac{\sigma'^2}{2} + \frac{\sigma'}{r} \right) - f_2' \left( \frac{\sigma'}{2} + \frac{1}{r} \right) - \frac{\eta' f_1'}{2} \\ & - \eta \left( f_1'' + \frac{\beta f_1'^2}{2} + \sigma' f_1' + \frac{f_1'}{r} \right) = 0. \end{aligned} \quad (36)$$

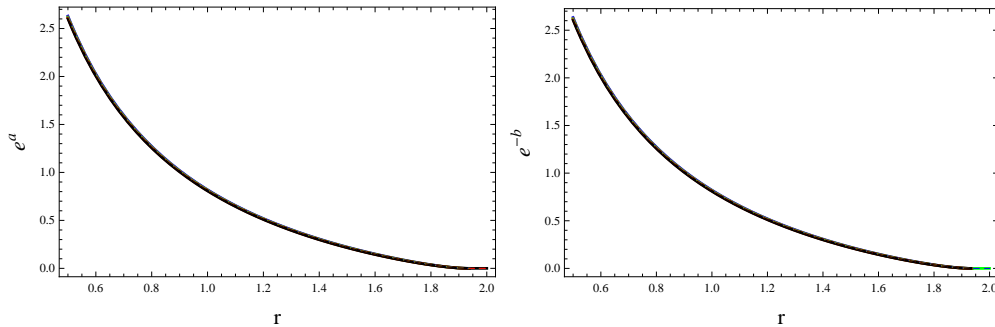


Figure 1: Graphs of deformed metric coefficients  $e^a$  and  $e^{-b}$  against  $r$  model I.

Using the equation above together with the relation given by Eq.(33), we obtain numerical approximations for the deformation functions  $f_1$  and  $f_2$ . Inserting these approximations of  $f_1$  and  $f_2$  in the EGD metric (31), we obtain our required solutions.

We present the graphs of the distorted metric, from which we analyze the asymptotic flatness of the obtained spacetime. A spacetime is termed as asymptotically flat if the metric potentials tend to 1 when the radial coordinate is taken to be sufficiently large. In such a spacetime, the effect of a gravitational field decreases and becomes unnoticeable after traveling a large distance from a gravitating body, thus the space outside this region looks almost flat. The Rastall and decoupling parameters  $\lambda = 0.01$  (solid lines),  $0.02$  (dashed lines), and  $\beta = -0.1$  (blue),  $-0.102$  (brown),  $-0.104$  (green),  $-0.106$  (red),  $-0.108$  (black) were used consistently in all calculations. We take  $M = 1$  as the mass, and this consideration contains an area that an observer can reach.

The plots of the deformed metric coefficients displayed in Figure 1 show that the resulting spacetime fails to preserve asymptotic flatness. We further plot the effective parameters (Figure 2) to describe the nature of our solution. The density turns out to be positive, while a positive radial pressure is obtained. Positive radial pressure means that there is an outward pressure opposing the inward pull of gravity. This is not a typical situation for a black hole because the strong gravitational forces inside a black hole are typically associated with very high inward pressure. However, in theoretical models involving unusual forms of matter or energy, like negative mass or energy, it is possible that there could be a positive radial pressure acting outward

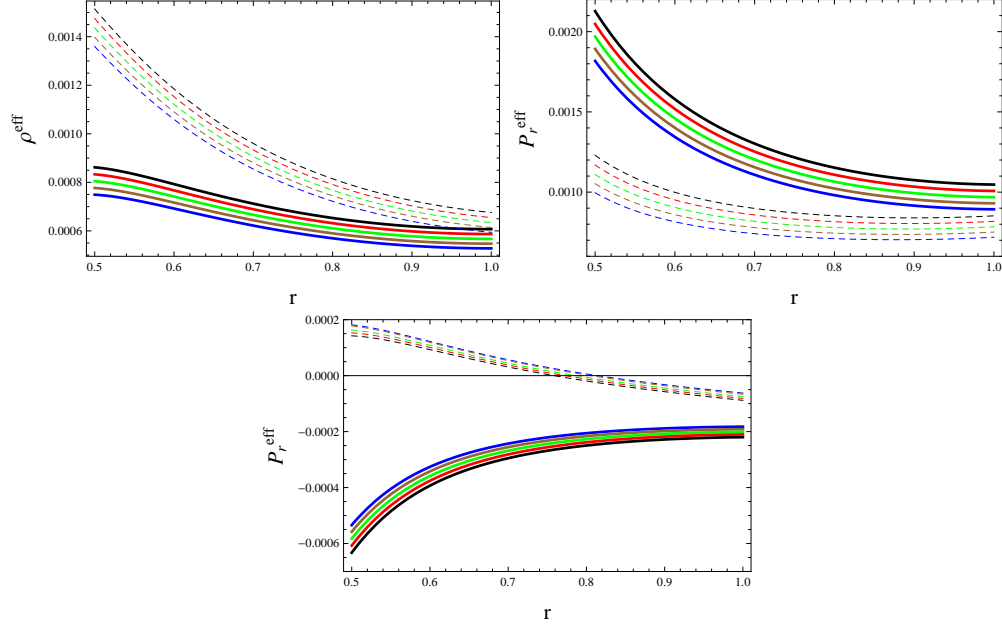


Figure 2: Graphs of  $\rho^{eff}$ ,  $P_r^{eff}$ ,  $P_t^{eff}$  against  $r$  for model I.

within the black hole. It is worthy to mention that a positive energy density could only be obtained for negative values of the decoupling parameter,  $\beta$ . With respect to the Rastall parameter ( $\lambda$ ), both the energy density and tangential pressure vary directly, while the radial pressure varies inversely. With regards to the decoupling parameter, the energy density and radial pressure vary inversely, while the tangential pressure varies directly.

It is interesting to observe that for both values of the Rastall parameter, the radial pressure is maximum around the core and monotonically decreases towards the event horizon. However, the lower value of the Rastall parameter ( $\lambda = 0.01$ ) induces a much higher pressure at the core. The difference in the radial pressures corresponding to the two Rastall parameters is thus more significant around the core while vanishing towards the surface. Similarly, the energy density is maximum at the core (for both values of the Rastall parameter) and decreases monotonically towards the surface. Contrary to the radial pressure, the higher value of the Rastall parameter ( $\lambda = 0.02$ ) induces a more dense core. As with the radial pressure, the difference in the densities (with respect to the two values of the Rastall parameter used) is greater around the core while disappearing towards the surface.

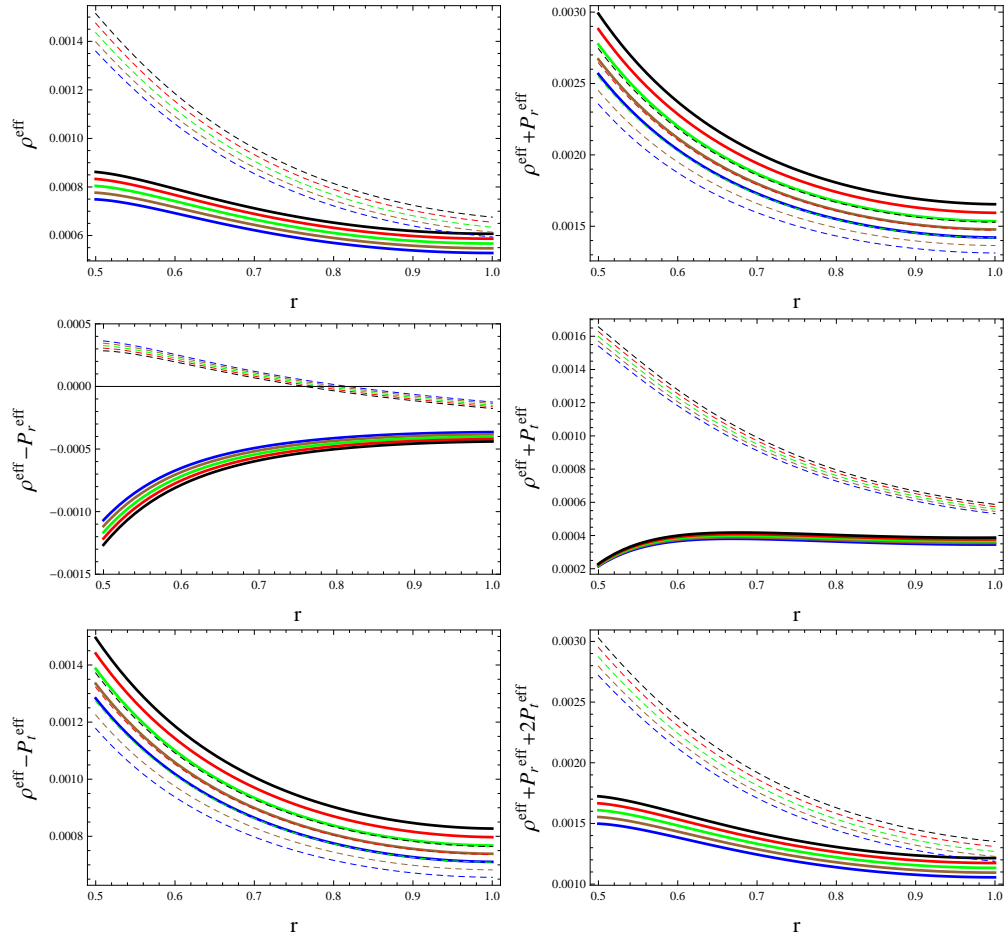


Figure 3: Graphs of energy bounds against  $r$  for model I.

Finally, we investigate the adherence of the thermodynamic variables to the following energy conditions

$$\begin{aligned}
\rho^{eff} &\geq 0, & \rho^{eff} + P_r^{eff} &\geq 0, \\
\rho^{eff} - P_r^{eff} &\geq 0, & \rho^{eff} - P_t^{eff} &\geq 0, \\
\rho^{eff} + P_t^{eff} &\geq 0, & \rho^{eff} + P_r^{eff} + 2P_t^{eff} &\geq 0.
\end{aligned} \tag{37}$$

These conditions, if satisfied, imply that the matter is ordinary. Failure to satisfy these energy conditions imply that the matter is exotic. The plots of the energy conditions in Figure 3 portray that the matter source is exotic, due to the violation of a dominant energy condition.

## 4.2 Model II: A barotropic EoS

The source  $\Theta_{ab}$  is termed as a polytropic fluid in the event if it satisfies the following EoS [30]

$$P_r^{eff} - \varrho \left( \rho^{eff} \right)^\Gamma, \tag{38}$$

where  $\varrho > 0$  contains parametric information about the temperature and  $\Gamma = 1 + \frac{1}{n}$ ,  $n$  is the polytropic index. Using the appropriate substitutions and considering the unique case  $\Gamma = 1$ , the equation above simplifies to

$$\varrho(\Theta_0^0) + \Theta_1^1 = 0, \tag{39}$$

denoting a barotropic EoS [30]. Equation (39) can be identified as a particular case of the EoS (34), with  $\alpha_1 = \frac{1}{\varrho}$  and  $\alpha_2 = 0$ . Using Eqs.(26) and (27), this equation gives

$$\begin{aligned}
& -\varrho \left( \frac{f_2'}{r} + \frac{f_2}{r^2} \right) - f_2 \left( \frac{\sigma'}{r} + \frac{1}{r^2} \right) - \frac{\eta f_1'}{r} + \frac{\lambda(\varrho + 1)}{4} \left[ f_2 \left( \sigma'' + \frac{\sigma'^2}{2} + \frac{2\sigma'}{r} \right) \right. \\
& \left. + f_2' \left( \frac{\sigma'}{2} + \frac{2}{r} \right) + \eta f_1'' + \eta \sigma' f_1' + \frac{\eta \beta f_1^2}{2} + \frac{\eta' f_1'}{2} + \frac{2\eta f_1'}{r} \right] = 0.
\end{aligned} \tag{40}$$

Using this equation together with Eq.(33), we obtain numerical approximations of the functions  $f_1$  and  $f_2$  which are then applied to the EGD metric (31) to obtain the required solution.

We plot the metric potentials in Figure 4 from which it is seen that the resulting spacetime is almost asymptotically flat, as the metric potentials

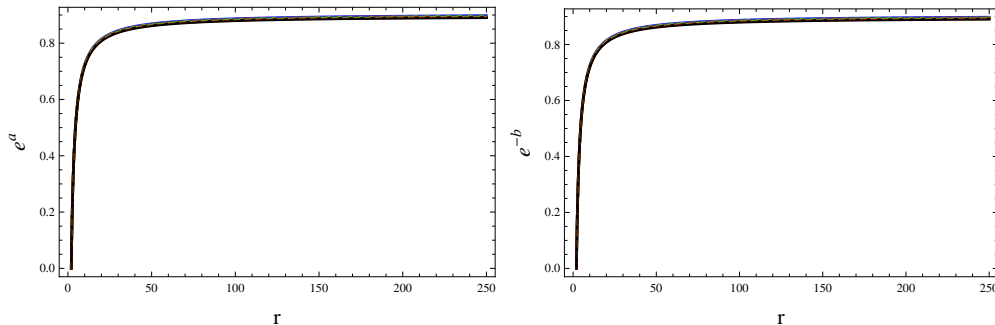


Figure 4: Graphs of deformed metric coefficients  $e^a$  and  $e^{-b}$  against  $r$  for Model II.

approach 0.9 (approximately 1) as  $r$  increases arbitrarily. The effective thermodynamic variables plotted in Figure 5, show a positive density, a negative radial pressure and a positive tangential pressure. An inward pressure is implied by a negative radial pressure, which strengthens the black hole's gravitational attraction. This idea is more consistent with the known information about black holes, where matter collapses to a singularity due to extremely high gravitational forces. In theoretical discussions, negative radial pressure is frequently used to explain phenomena such as the universe's accelerated expansion in theories including dark energy with negative pressure. It is observed that the increment in the Rastall parameter registers no significance in the outputs of the energy density and radial pressure. This increment, however, induces a higher tangential pressure. Both energy density and tangential pressure are maximum at the core and decrease monotonically towards the surface. To the contrary, the radial pressure is minimum at the core and increases monotonically towards the surface. With respect to the decoupling parameter, the density and tangential pressure vary inversely while the radial pressure vary directly. Finally, the analysis of the energy conditions in Figure 6 reveals an exotic source due to the violation of one of the dominant energy conditions.

### 4.3 Model III: A Particular Case

We consider a unique case of the EoS (34) with  $\alpha_1 = 1.4$  and  $\alpha_2 = -3$  as in [30], thus giving the linear equation

$$\Theta_0^0 + 1.4\Theta_1^1 + 3\Theta_2^2 = 0. \quad (41)$$

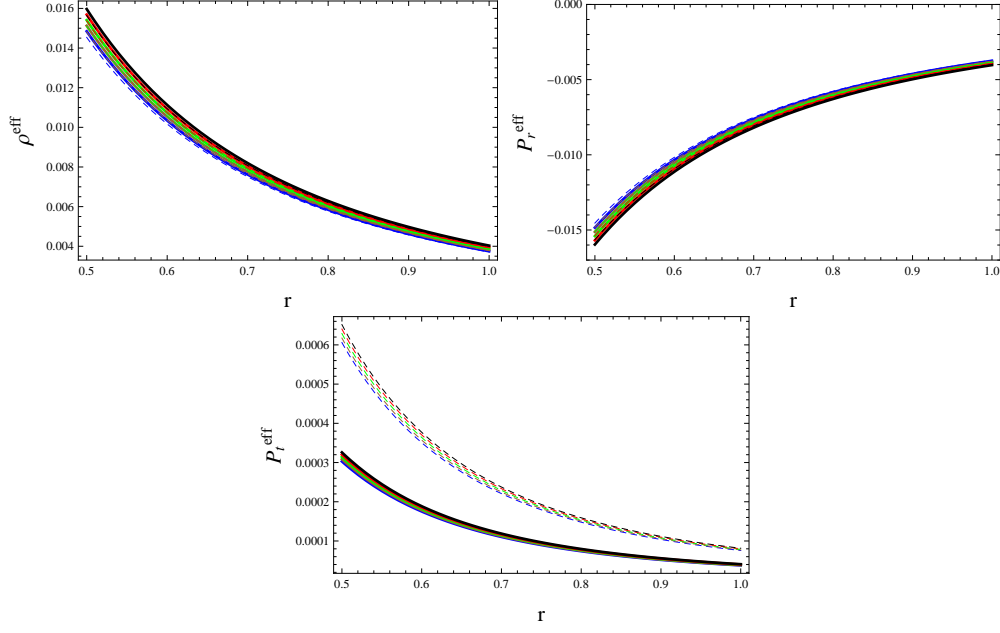


Figure 5: Graphs of  $\rho^{eff}$ ,  $P_r^{eff}$ ,  $P_t^{eff}$  against  $r$  for model II.

This equation leads to

$$\begin{aligned}
& -3f_2 \left( \frac{\sigma''}{2} + \frac{\sigma'^2}{4} + \frac{\sigma'}{2r} \right) - \frac{3\sigma'f_1'}{4} - 3\eta \left( \frac{f_1''}{2} + \frac{\beta f_1'^2}{4} + \frac{\sigma'f_1'}{2} + \frac{f_1'}{2r} \right) \\
& + \frac{\lambda}{4} \left[ f_2 \left( \sigma'' + \frac{\sigma'^2}{2} + \frac{2\sigma'}{r} \right) + f_2' \left( \frac{\sigma'}{2} + \frac{2}{r} \right) + \eta f_1'' + \eta \sigma' f_1' + \frac{\eta \beta f_1'^2}{2} + \frac{\eta' f_1'}{2} \right. \\
& \left. + \frac{2\eta f_1'}{r} \right] - \frac{f_2'}{r} - \frac{f_2}{r^2} - 1.4f_2 \left( \frac{\sigma'}{r} + \frac{1}{r^2} \right) - \frac{1.4\eta f_1'}{r} - 3f_2' \left( \frac{\sigma'}{4} + \frac{1}{2r} \right) = 0.
\end{aligned} \tag{42}$$

As with the cases of the previously obtained models, we use the equation above together with the relation given by Eq.(33) to obtain the functions  $f_1$  and  $f_2$ . The metric for the spacetime describing the obtained black hole can then be evaluated by using these functions in the EGD metric (31). Figure 7 shows the plots of the metric potentials which show that the resulting spacetime is not asymptotically flat. The effective thermodynamic variables are shown in Figure 8. A positive energy density and a negative tangential pressure are observed, both of which vary directly with the Rastall parameter.



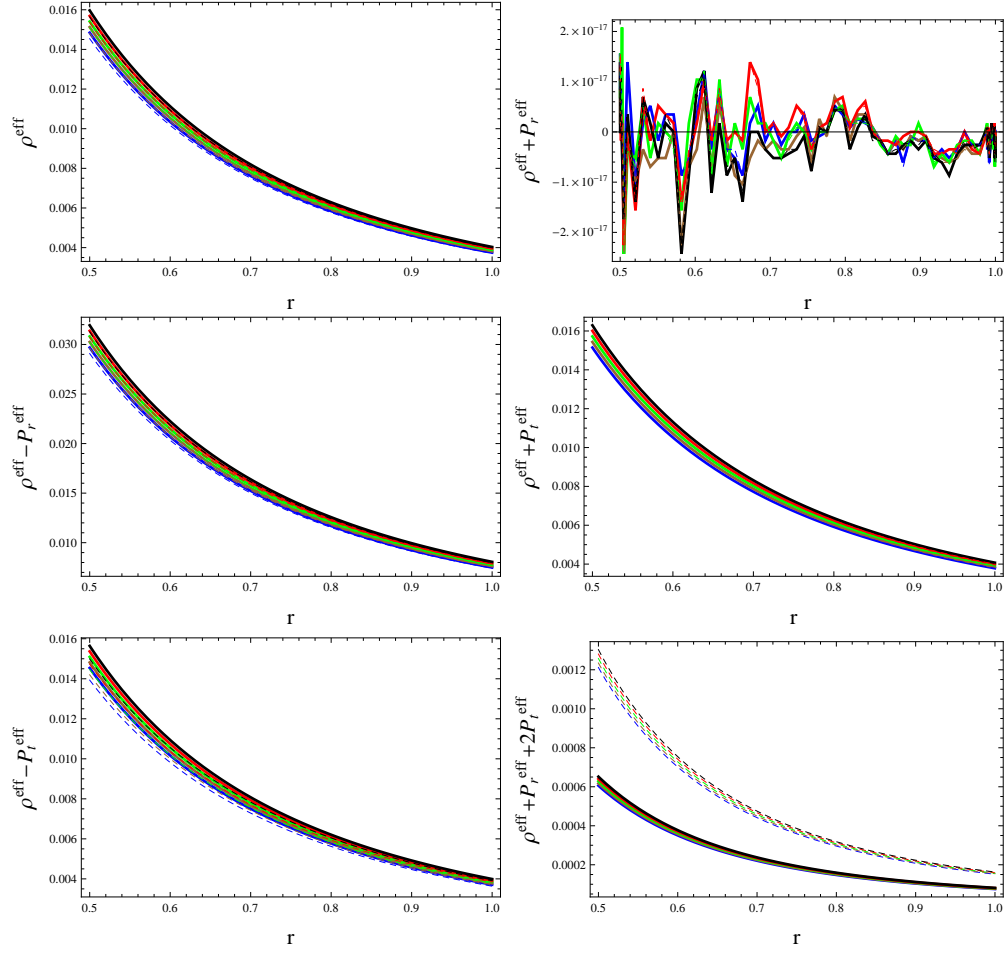


Figure 6: Graphs of energy bounds against  $r$  for model II.

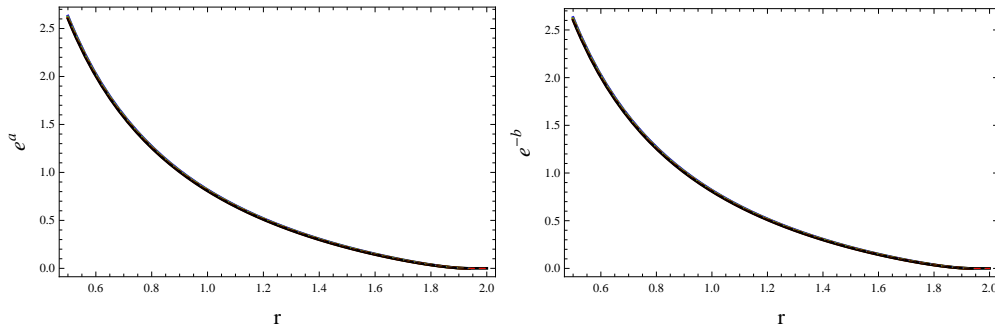


Figure 7: Graphs of deformed metric coefficients  $e^a$  and  $e^{-b}$  against  $r$  for model III.

The radial pressure turns out to be positive and varies inversely with the Rastall parameter. The decoupling parameter, however, varies inversely with the energy density and radial pressure, while exhibiting direct proportionality to the tangential pressure. It can be observed for this model that the variation of the Rastall parameter registers a significant difference in the output of all three thermodynamic variables. Lastly, we plot the energy conditions which again show a violation of some dominant conditions (Figure 9).

## 5 Conclusions

This paper focuses on exploring the EGD method to extend the known Schwarzschild black hole solution within the framework of the Rastall theory of gravity. The field equations for an extra matter source gravitationally coupled to a seed source of matter are explicitly formulated. Under the EGD strategy, no restrictions are made with regards to the nature of the interaction between the coupled matter sources. These field equations are extensively decoupled, thus generating two new systems which correspond to the seed and extra source, respectively. This decoupling has been done via linear transformations which alters both metric coefficients.

Due to the presence of a vacuum (which characterizes the seed source), the obtained models are explicitly described by the extra source,  $\Theta_{ab}$ . We have thus obtained the extended models by imposing two appropriate constraints on the metric functions and on this extra source. The first constraint ( $a = -b$ ) which is imposed on the metric functions ensures that the Killing and causal horizons overlap, which is a necessary prerequisite

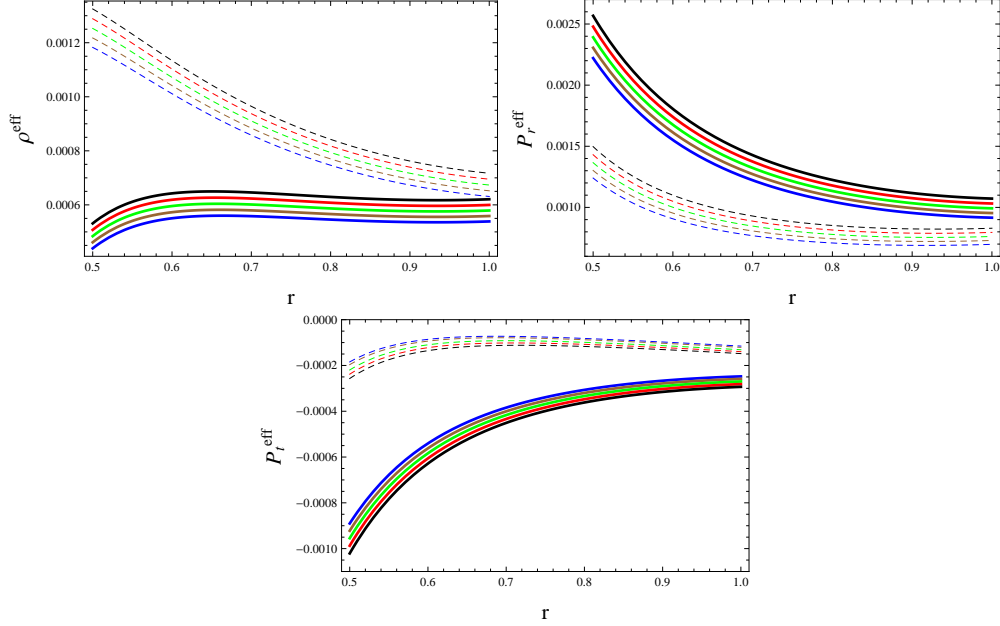


Figure 8: Graphs of  $\rho^{eff}$ ,  $P_r^{eff}$ ,  $P_t^{eff}$  against  $r$  for model III.

for a well defined black hole model. The second constraint is given by the linear EoS,  $\Theta_0^0 + \alpha_1 \Theta_1^1 = \alpha_2 \Theta_2^2$ , through which the extended models are obtained. Three models corresponding to three cases of the mentioned EoS are thus obtained. The effect of the Rastall and decoupling parameters, respectively, have been extensively investigated for all the obtained models. To this effect, we have adopted the values  $\lambda = 0.01, 0.02$  and  $\beta = -0.1, -0.102, -0.104, -0.106, -0.108$ . It is found that increasing the Rastall parameter induces a denser core in models I and III, while no effect is registered in model II. With regard to the radial pressure, the effect of this increment marks a lower radial pressure.

For all the obtained models, the energy density is found to be positive, as required. A negative radial pressure (which is typical for black holes) is only obtained for the second model given by a barotropic EoS (41). It is worthy to mention that all the three cases considered in this work are also considered in GR [30] and BD theory [38]. However, with regards to the behavior of the thermodynamic variables, only the results of model II are in line with the results of their counterparts in [31, 38]. Through analysis of the metric potentials, it is found that only the second model tends to an asymptotically

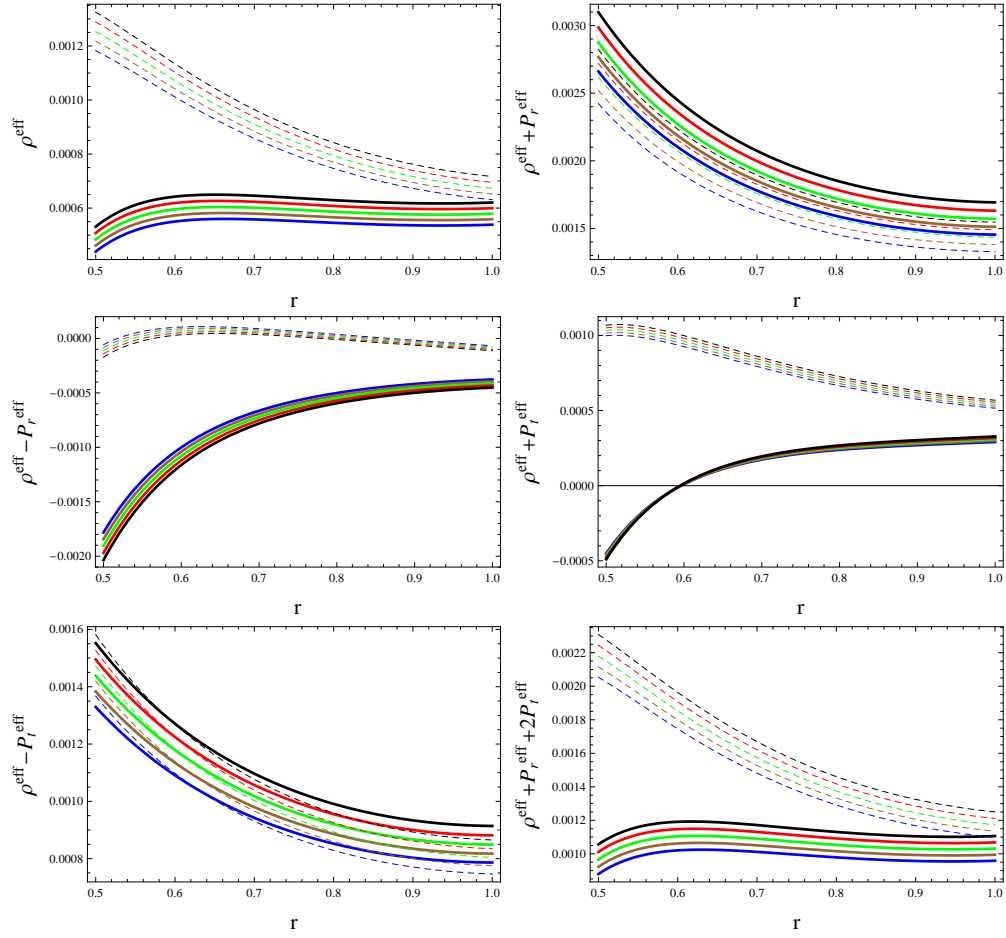


Figure 9: Graphs of energy bounds against  $r$  for  $\lambda = 0.01$  (solid),  $0.02$  (dashed),  $\beta = -0.1$  (blue),  $-0.102$  (brown),  $-0.104$  (green),  $-0.106$  (red) and  $-0.108$  (black) for model III.

flat spacetime. In GR [31], the model obtained from the traceless extra source (corresponding to our model I) failed to preserve asymptotic flatness. In BD theory [38], however, it was found that only the model generated using a barotropic EoS (corresponding to our model II) failed to preserve asymptotic flatness.

It is found for all obtained models that the dominant energy conditions are not satisfied, implying that the additional source is exotic in all cases. This result was also obtained in GR [30], where it was concluded that the dominant energy conditions are unsatisfiable using the EoS (34). The metric potential (Figures 1, 4 and 7) reveal that all the obtained models have Killing and causal horizons coinciding at  $r = 2M$ , where ( $M = 1$ ). Another observation directed at the EGD metric (31), reveals that all the extended models have a singularity at  $r = 0$ . Thus putting together these two aforementioned observations drive us to the conclusion that all the obtained models have a singularity at  $r = 0$  hidden behind the horizon at  $r = 2M$ . This result is common to [31] and [38].

**Data Availability Statement:** No data was used for the research described in this paper.

## References

- [1] Rastall, P.: Phys. Rev. D **6**(1972)3357.
- [2] Moradpour, H., Heydarzade, Y., Darabi, F. and Salako, I.G.: Eur. Phys. J. C **77**(2017)259.
- [3] Josset, T. and Perez, A.: Phys. Rev. Lett. **118**(2017)021102.
- [4] Ma, M.S. and Zhao, R.: Eur. Phys. J. C **77**(2017)629.
- [5] Bezerra de Mello, E.R., Fabris, J.C. and Hartmann, B.: Class. Quantum Grav. **32**(2015)085009.
- [6] Oliveira, A.M., Velten, H.E.S., Fabris J.C. and Casarini, L.: Phys. Rev. D **92**(2015)044020; *ibid.* **93**(2016)124020.
- [7] Bronnikov, K.A., Fabris, J.C., Piattella, O.F. and Santos, E.C.: Gen. Relativ. Gravit. **48**(2016)162.

- [8] Licata, I., Moradpour, H. and Corda, C.: *Int. J. Geom. Methods Mod. Phys.* **14**(2017)1730003.
- [9] Capone, M., Cardone, V.F. and Ruggiero, M.L.: *Nuovo Cim. B* **125**(2011)1133.
- [10] Batista, C.E.M. et al.: *Phys. Rev. D* **85**(2012)084008.
- [11] G. F. Silva, G.F. et al.: *Grav. Cosmol.* **19**(2013)156.
- [12] Santos, A.F. and Ulhoa, S.C.: *Mod. Phys. Lett. A* **30**(2015)1550039.
- [13] Moradpour, H.: *Phys. Lett. B* **757**(2016)187.
- [14] Abbott, B.P. et al.: *Phys. Rev. Lett.* **116**(2016)061102.
- [15] Akiyama, K. et al.: *Astrophys. J.* **875**(2019)L1.
- [16] Heydarzade, Y., Moradpour, H. and Darabi, F.: *Can. J. Phys.* **95**(2017)1253.
- [17] Kumar, R. and Ghosh, S.G.: *Eur. Phys. J. C* **78**(2018)750.
- [18] Lobo, I.P. et al.: *Int. J. Mod. Phys. D* **27**(2018)1850069.
- [19] Ovalle, J.: *Phys. Rev. D* **95**(2017)104019.
- [20] Morales, E. and Tello-Ortiz, F.: *Eur. Phys. J. C* **78**(2018)841.
- [21] Tello-Ortiz, F. et al.: *Eur. Phys. J. C* **79**(2019)885.
- [22] da Rocha, R.: *Eur. Phys. J. C* **81**(2021)845; *ibid.* **82**(2022)34.
- [23] Maurya, S.K. et al.: *Eur. Phys. J. C* **83**(2023)317.
- [24] Rehman, H. and Abbas, G.: *Chin. Phys. C* **47**(2023)125106.
- [25] Sharif, M. and Waseem, A.: *Chin. J. Phys.* **60**(2019)426; *Ann. Phys.* **405**(2019)14; Sharif, M. and Majid, A.: *Chin. J. Phys.* **68**(2020)406; *Phys. Dark Universe* **30**(2020)100610; Sharif, M. and Saba, S.: *Chin. J. Phys.* **63**(2020)348; *Int. J. Mod. Phys. D* **29**(2020)2050041.
- [26] Casadio, R., Ovalle, J. and da Rocha, R.: *Class. Quantum Grav.* **32**(2015)215020.

- [27] Ovalle, J., Casadio, R., da Rocha, R. and Sotomayor, A.: Eur. Phys. J. C **78**(2018)122; Sharif, M. and Sadiq, S.: Eur. Phys. J. C **78**(2018)410.
- [28] Sharif, M. and Naseer, T.: Chin. J. Phys. **73**(2021)179; Universe **8**(2022)62; Sharif, M. and Hassan, K.: Eur. Phys. J. Plus **137**(2022)997; Universe **9**(2023)165.
- [29] Sharif, M. and Sallah, M.: New Astron. **109**(2024)102198; Eur. Phys. J. Plus **139**(2024)819.
- [30] Sharif, M. and Sallah, M.: Phys. Scr. **99**(2024)115031; Chin. J. Phys. **92**(2024)794.
- [31] Ovalle, J. et al.: Eur. Phys. J. C **78**(2018)960.
- [32] Ovalle, J.: Phys. Lett. B **788**(2019)213.
- [33] Contreras, E. and Bargueño, P.: Class. Quantum Grav. **36**(2019)215009.
- [34] Sharif, M. and Ama-Tul-Mughani, Q.: Ann. Phys. **415**(2020)168122.
- [35] Sharif, M. and Majid, A.: Phys. Dark Universe **30**(2020)100610.
- [36] Ovalle, J. et al.: Phys. Dark Universe **31**(2021)100744.
- [37] Sharif, M. and Majid, A.: Phys. Dark Universe **32**(2021)100803.
- [38] Sharif, M. and Majid, A.: Phys. Scr. **96**(2021)035002.
- [39] Sharif, M. and Naseer, T.: Indian J. Phys. **96**(2022)4373; Int. J. Mod. Phys. D **31**(2022)2240017.
- [40] Sharif, M. and Naseer, T.: Class. Quantum Grav. **40**(2023)035009.
- [41] Sharif, M. and Naseer, T.: Chin. J. Phys. **86**(2023)596; Eur. Phys. J. Plus **139**(2024)86.